Dzwinel, W., Complex automata as a novel conceptual framework for modeling biomedical phenomena, Byrski, A.; Oplatkova, Z.; Carvalho, M.; Dorohnicki, M.K. (Eds.), in Studies in Computational Intelligence, Advances of Intelligent Modelling and Simulation, Springer Verlag, Vol. 416/2012, 269-298, DOI: 10.1007/978-3-642-28888-3_11, 2012

Complex automata as a novel conceptual framework for modeling biomedical phenomena*

Witold Dzwinel

Department of Computer Science
AGH University of Science and Technology
Al. Mickiewicza 30, 30-059 Kraków, Poland
dzwinel@agh.edu.pl

Abstract

We show that the complex automata (CxA) paradigm can serve as a robust general framework which can be applied for developing advanced models of biological systems. CxA integrates particle method (PM) and cellular automata (CA) computational techniques. Instead of developing complicated multi-scale models which consist of many submodels representing various scales coupled by a scales-bridging mechanism, we propose here a uniform, single scale, coarse grained computational framework for which information about finer scales is inscribed in CA rules and particle interactions. We demonstrate that our approach can be especially attractive for modeling biological systems, e.g., intrinsically complex phenomena of growth such as cancer proliferation fueled by the process of angiogenesis and *Fusarium Graminearum* wheat infection. We show that these systems can be discretized and represented by an ensemble of moving particles, which states are defined by a finite set of attributes. The particles may represent spherical cells and other non-spherical fragments of more sophisticated structures, such as, transportation system (vasculature, capillaries), pathogen individuals, neural network fragments etc. The particles interact with their closest neighbors *via* semi-harmonic central forces mimicking mechanical resistance of the cell walls. The particle motion is governed by both the Newtonian laws and cellular automata rules employing the attributes (states) of neighboring cells. CA rules may reflect e.g., cell life-cycle influenced by accompanying biological processes while the laws of particle dynamics and the character of collision operators simulate the mechanical properties of the system. The ability of mimicking mechanical interactions of tumor with the rest of tissue and penetration properties of *Fusarium graminearum,* confirms that our model can reproduce realistic 3-D dynamics of these complex biological systems.

Keywords: particle method, cellular automata, complex automata, modeling, tumor growth, *Fusarium Graminearum* proliferation, fluid flow, parallel computing

* based on the invited talk presented on 2nd International Conference on Computational Engineering (ICCE 2011), Darmstadt, 4-6 October 2011

1. Introduction

New challenges in systems biology involve searching for new modeling paradigms which allow for simulating multi-scale systems within a unified framework. As shown in Fig.1, the multi-scale simulations are large-scale simulations involving many spatio-temporal scales and many heterogeneous modeling approaches.

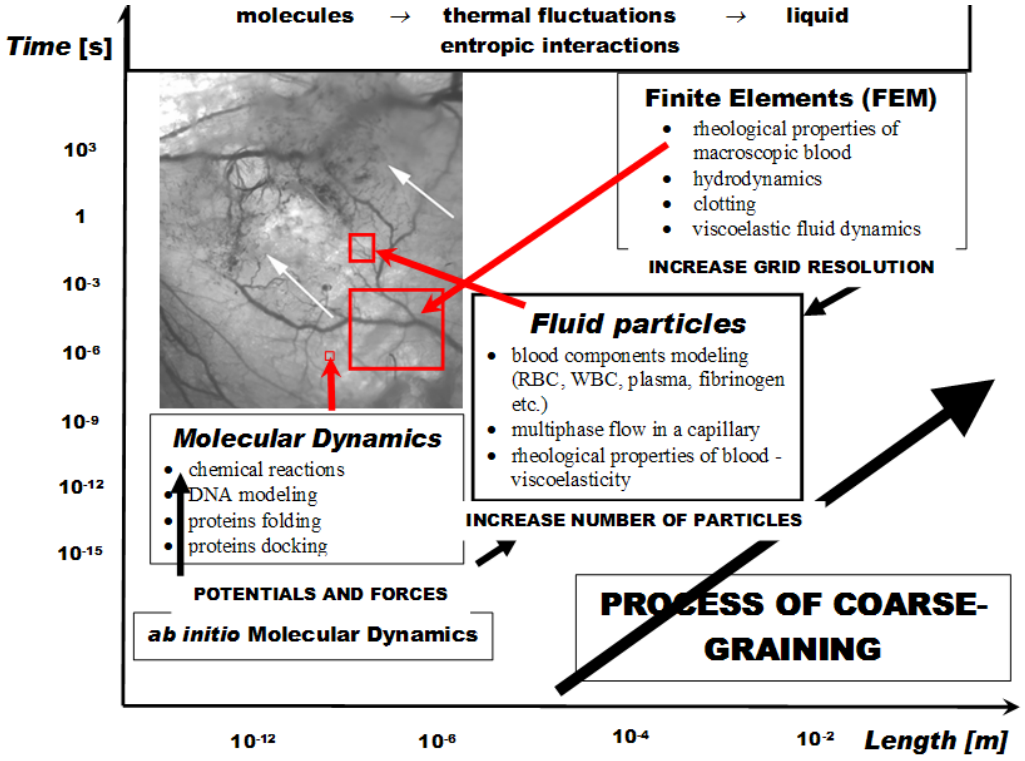

Fig.1. The scale separation diagram of blood system involving multiple scales and various computational models [1].

This fact poses at least two serious problems. The first one refers to matching and bridging heterogeneous models representing different scales (e.g. discrete and continuum), while the second one, is connected with merging different parallelization strategies. Moreover, the common strategy of continuum and discrete models bridging by running finer scale models only in the region of interest (ROI) involving more degrees of freedom (see Fig.2), may fail for biological systems, where coupling between fine and coarser scales can be very tight. This may cause that the finest spatio-temporal scales will still decide about the computational complexity despite the existence of well separated coarse grained modes.

The interesting alternative to the continuous/discrete approaches is the development of a universal computational framework, which could be matched to the following spatio-temporal scales through the process of successive coarse graining. It can be understood as a numerical equivalent of some renormalization procedures used from many years in physics for simplification of formal mathematical models. Thus the successive coarse graining can be defined as the approximation process limiting the number of DoF (degrees of freedom) and the frequency of their motion starting from the smallest to the largest scales of interest.

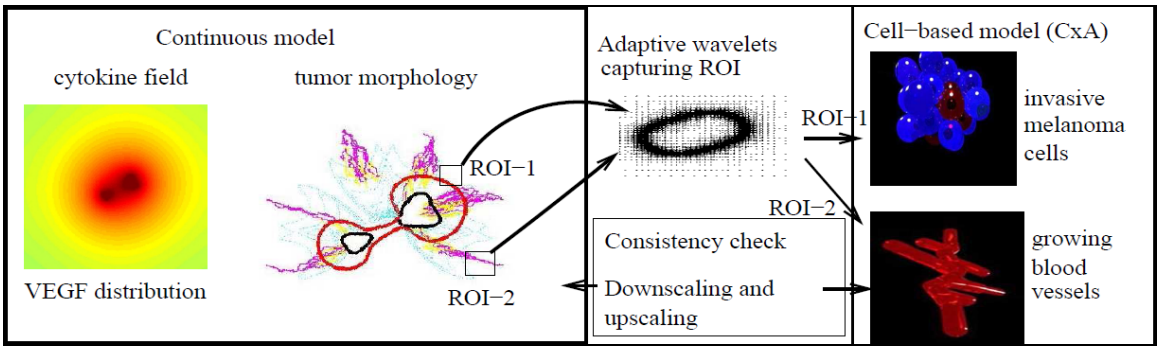

Fig.2. The continuous model treats macroscopic tumor morphology and cytokine distribution fields. The cell-based model handles individual cell proliferation and motion and is only applied in Regions of Interest (RPI). The connection between two models is made by the adaptive wavelets [2] which are far denser in ROI [3].

Signal decomposition and multiresolution are good metaphors of the notions of successive coarse graining and multi-scaling. The principles of signal decomposition are demonstrated in Fig.3.

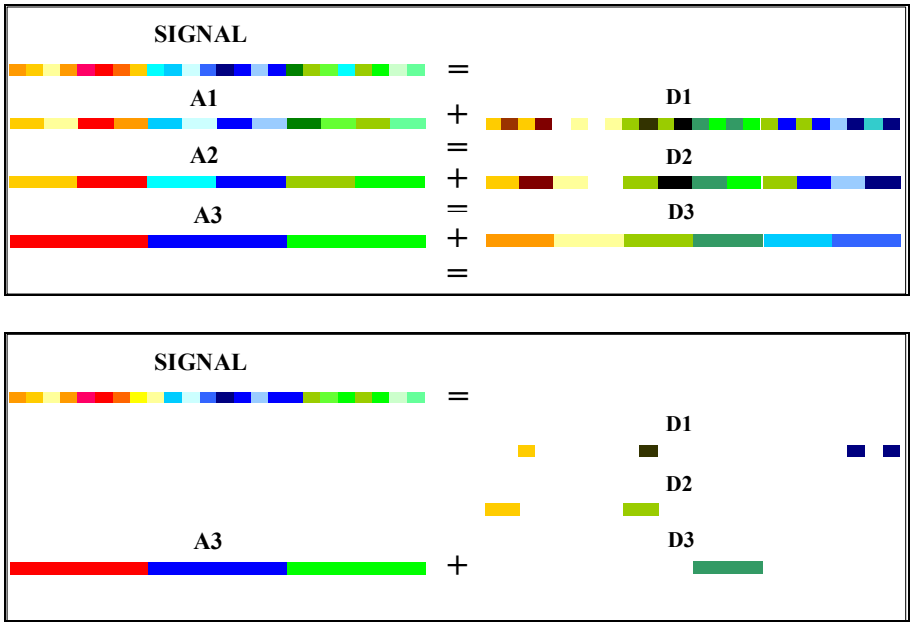

Fig.3 The upper panel represents signal decomposition onto approximation (A) and details (D) on various resolution levels (1-3). The signal is equal to the sum of approximation on a given level and all the details from the finest levels (e.g. SIGNAL=A3+D3+D2+D1). As shown in the bottom panel, eliminating the least important details, the signal can be reconstructed using approximation (A3) and only a fraction of the most important details from the finer scales.

Every signal can be decomposed onto approximations (A) and details (D) on successive resolution levels using a set of basis functions with compact support (such as wavelets, RBF etc.).
Then, the signal is equal to the sum of approximation on a given resolution level and all the details from the finest levels. By cutting off the least important details, i.e. all of these having the weights below a certain threshold, the signal can be reconstructed using approximation (A3) and only a fraction of the most important details from the finer resolutions. This brings about the question of how this smart method can be applied in developing multi-scale models.

To find the analogies between signal decomposition and developing multi-scale models we should define first a homogeneous computational environment, which allows for defining principal modeling procedures in the scope of the same conceptual framework. We consider here two computational frameworks, namely, cellular automata and particle method.

Cellular automata (CA) paradigm is a simplistic model of computation. The seminal Wolfram's book "New Kind of Science" [4] advocates that CA paradigm can be treated as a universal paradigm and a metaphor of reality. Cellular automata model is very compact and elegant indeed. CA is defined as a triple CA = (a(t),S_A, f_A). It consists of a complete number N_R of update rules f_A, which govern the deterministic evolution of a lattice of CA states a(t) in a discrete time t. The states are labeled by a finite alphabet $\{S_A\}$. For the simplest 1-D: CA → S_A=$\{0,1\}$, and the update rule f_A is a function of the closest neighbors only f_A: $\{S_A\}^3 \rightarrow \{S_A\}$ $\wedge$ $a_n(t+1) = f_A [a_{n-1}(t) , a_n(t) , a_{n+1}(t)]$. The number of rules is strictly limited, i.e. $N_R = \sum_{i=0,7} 2^i \cdot \alpha_i$ = 256, $\alpha_i \in \{0,1\}$. The transition principles are shown in the figure below.

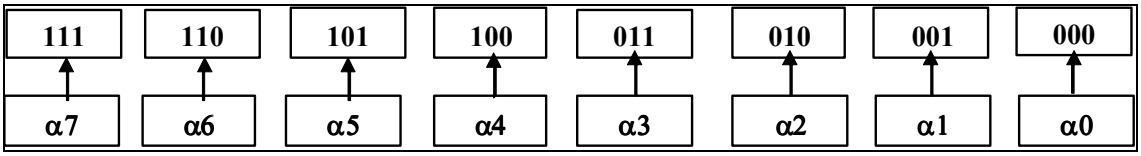

This way, every transition rule has its unique number from 0…255. The number of possible rules increases with growing alphabet, the number of neighbors and dimensionality of the CA environment.

The scope of CA applications is very broad, ranging from microscopic to macroscopic phenomena (e.g., [4,5]). So, the natural question is whether the CA paradigm represents truly multi-scale properties allowing for development coarser CA models through approximation of the finer ones.

In the first section of this paper we address two important issues:

1. How to construct the coarse graining procedure to retain physically important information from smaller scales?
2. What type of CA can/cannot be coarse grained?

We postulate, according to the results obtained by Israeli and Goldenfeld [6], a general principle of coarse graining which can reflect the signal decomposition procedure from Fig.3. Then we discuss its usefulness in coarse graining of very different computational framework, namely, Particle Model (PM).

The robustness of CA is still qualitative - metaphoric. Although some CA clones such as lattice gas and lattice Boltzmann gas [5], are able to describe many dynamical properties of physical systems, they simulate mechanical interaction, such as inertia, in a very simplistic and counterintuitive way. This is unlike another broadly used modeling tool – the model of interacting particles or Particle Model (called also Particle Method or Discrete Element Method (DEM) (e.g. [7,8,9,10]) for which mechanical interactions are its intrinsic property. The Particle Model is a discrete, off-grid and very general paradigm of modeling, which has its roots in N-body modeling and well known Molecular Dynamics (MD) method (also the Non-equilibrium Molecular Dynamics NEMD). Its broad scope of application was described in [1]. The principles of the method are shown in Fig.4.

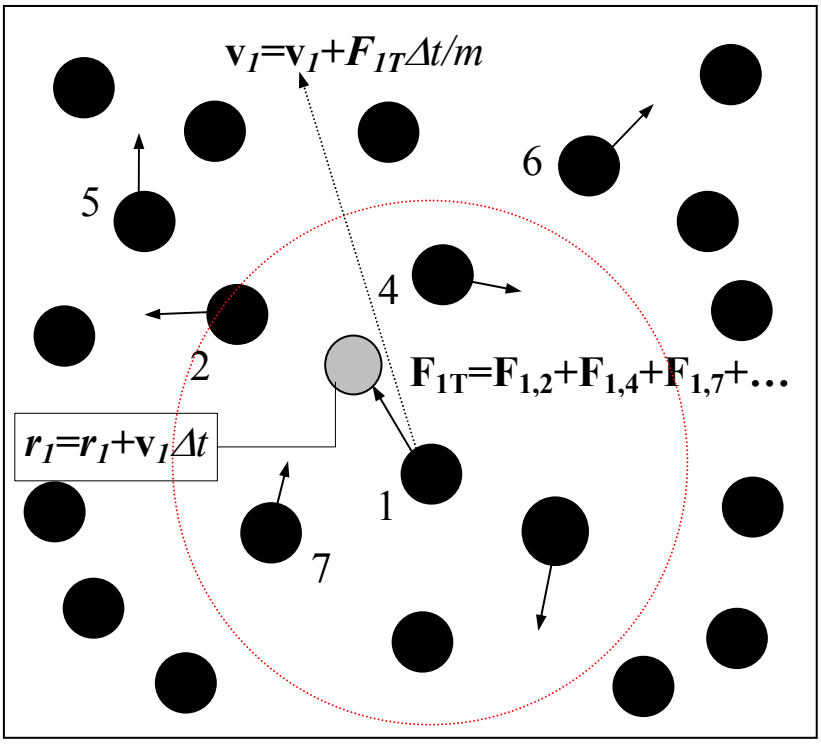

Fig.4 The diagram presenting principles of Particle Method

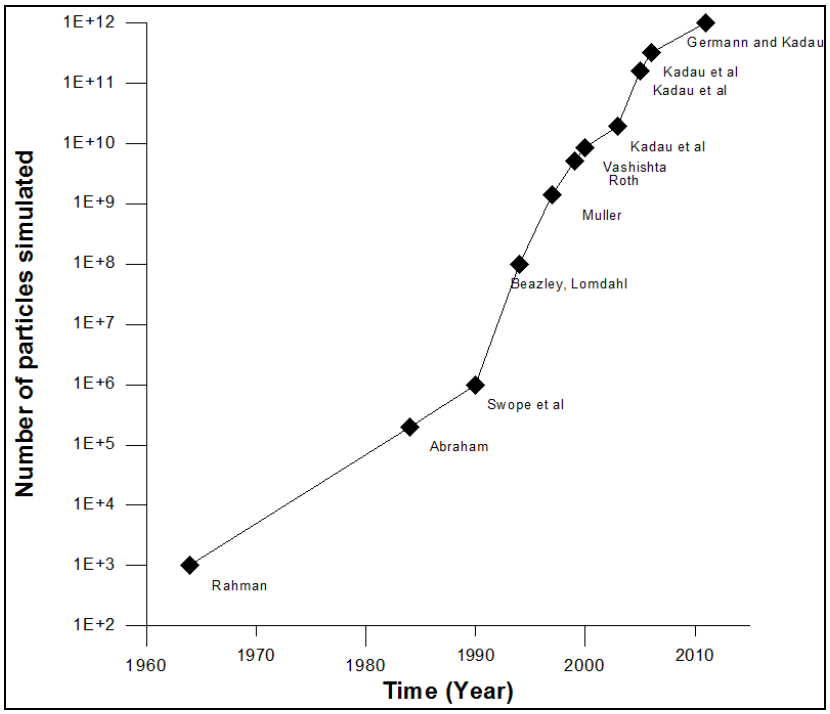

Fig.5. The plot displaying the history of the state_of_the_art high performance MD simulations. The abrupt speed-up after year 1990 is the result of development of efficient MD parallel codes (Beazley and Lomdahl, 1996 [11] – on TMCM5 1024 processor) and development of a new paradigm of the Non-Equilibrium Molecular Dynamics (se e.g.[1,12]).

The system of discrete particles is defined by boundary and initial conditions and by interactions between particles represented by a collision operator $\boldsymbol{\Omega}_{ij}$. The particle system evolves according to the Newtonian equations of motion, which can be described in a discrete form as follows:

$$\Delta \mathbf{P}_i^n = \sum_j^N \mathbf{\Omega}_{ij} \cdot \mathbf{e}_{ij}^n \Delta t, \qquad \Delta \mathbf{r}_i^n = \frac{\mathbf{P}_i^n}{m} \Delta t \,, \tag{1}$$

where $\mathbf{r}_i$ is the position of particle, $\mathbf{P}_i$ is its momentum and Δt the integration time-step, N is the number of particles in the interaction range.

As shown in Fig.5, the state_of_the_art supercomputers allow for simulating more than a trillion atoms in a million time-steps using highly efficient MD parallel codes [13]. This particle ensemble corresponds to spatial 3-D scales of a few micrometers and time scales of ten nanoseconds. This may suggest that the particle approach is not appropriate for simulating larger systems due to high computational demands.

However, as shown in (e.g.,[1, 7, 14, 15]), Molecular Dynamics can be used as an efficient modeling framework also in larger scales. It appears that the spatio-temporal scale under interest depends on the definition of particle (quark, atom, molecule, granule, cluster, chunk of matter, object, individual, the planet, galaxy etc.) and the type of particle-particle interactions (hard/soft: long/short range, central/ non-central, two-body/many-body, dissipative/ conservative, stochastic/ deterministic etc.) [1,14]. Thus the definition of particle and the respective type of particle-particle interactions can be treated as the results of a successive coarse graining procedure. However, such the procedure cannot be as precisely defined as it is for cellular automata.

The main weakness of the particle model is the difficulty to represent important microscopic degrees of freedom in the form of particle interactions. For example, modeling crowd dynamics using only the metaphor of mechanical collisions of particles [15,16] (where a particle corresponds to an individual) can neglect some important "microscopic" phenomena such as development of panic, anger, falls and blockage due to local crush etc.. Even if some of these factors can be represented by a sort of stochastic force (such as panic factor in [16]), additional thresholding conditions dependent on the current properties of neighboring individuals should be arbitrary defined. The problem becomes even more acute in modeling biological systems. Assuming that a particle represents a cell, the microscopic processes such as chemical signaling, chemotaxis, haptotaxis, oxygen and proteins diffusion influencing cell behavior and its functions cannot be mimicked by a simple mechanical force. On the other hand, just mechanical interactions between cells can be a crucial factor for some type of growth, such as solid cancer proliferation.

In [17] the authors propose complex automata (CxA) model as a multiscale paradigm consisting of a set of single scale CA representing processes operating on different spatio-temporal scales. The authors define adequate coupling templates between the scales to model and simulate multi-scale phenomena. The CA considered are typically based on the Lattice Boltzmann Models (LBM) [5]. Besides generalized CA to represent single scale models, the CxA approach also includes Agent Based Models (ABM) [17].

Our approach is different. Instead of developing multi-scale model which consists of many submodels representing various scales coupled by a scale-bridging mechanism, we propose a uniform coarse grained model in which information about finer scales is inscribed in CA rules and particle interactions. In the following section we demonstrate that by coupling cellular automata and particle model we can develop a new computational framework which possesses the advantages of the two. By using as examples two modeling targets: proliferation of cancer and invasion of *Fusarium Graminearum* – a pathogen attacking cereal crops - we demonstrate how the concept of complex automata woks in modeling realistic phenomena. In the conclusions we propose some validation issues for CxA model.

2. Coarse graining

2.1. Cellular automata

The concept of coarse-graining has been introduced to cellular automata by Israeli and Goldenfarb in [6]. Let us the original CA be defined as $A = (a(t),S_A, f_A)$ and its coarse-graining equivalent $B = (b(t),S_B, f_B)$. The projection (or mapping) function P: $S_A^N \rightarrow S_B$ will

be used to map the block of N cells from A into exactly one cell of B. The block of N cells from A, A^N, is called a supercell. Then the condition that has to be satisfied by automata B and projection function P in order to provide coarse-graining of A is as follows:

$$P \cdot \underbrace{f_A \cdot \ldots \cdot f_A}_{N} \cdot a = f_B \cdot P \cdot a \tag{2}$$

Where P·a denotes that the whole lattice a is divided onto blocks of size N, and then we apply projection P for each block separately. The notation $f_A \cdot a$ means, that we apply the local transformation f_A of automata A to every cell in the lattice a. The expression (2) says, that running automata A for N times and mapping the result using P, gives the same final CA configuration as applying P at first, and then running automata B only once. This has to be satisfied for any starting configurations of A.

In [6] Israeli and Goldenfarb show a simple procedure for finding coarse grained configuration of a given automata. This very inefficient procedure has to be described in order to understand some basic properties of coarse graining of cellular automata. Let us define the N'th supercell automata as:

$$A_N = \left(a^N(t), S_A^N, f_{A^N}\right) \tag{3}$$

This new automata operates over blocks of N cells from a(t) lattice. Let us consider 1-dimentional automata with neighborhood of size k=3. The local function f_{A^N} is then f_{A^N} : $\{S^N\}^3 \rightarrow S^N$. We can compute easily the value of f_{A^N} for some $x \in \{S^N\}^3$. This could be done by converting x into 3N-element lattice of automata A, and running automata A exactly N times:

$$y = \underbrace{f_A \cdot \ldots \cdot f_A}_{N} \cdot x\,. \tag{4}$$

Now we may also choose the alphabet of coarse grained automata B to fit into the alphabet of A_N:

$$S_B \subseteq S_{A^N} \tag{5}$$

Since there is a nonsense to consider S_B to be larger than $(\#S_A)^N$. That is because for $S_B \equiv S_{A^N}$ mapping function $P(.)$ is injective, and we would not have any benefits using larger alphabet. Utilizing all given definitions (see Eq.(2)), we could rewrite the rule that need to be satisfied by coarse-grained automata B and its local function:

$$f_B\left[P(x_1); P(x_2); P(x_3)\right] = P\left(f_{A^N}\left[x_1; x_2; x_3\right]\right) \tag{6}$$

We need to keep in mind, that $P(.)$ does not has to be injective, and there is a possibility that $(P(y_1);P(y_2);P(y_3))=(P(x_1);P(x_2);P(x_3))$ for another triple of N-element blocks $(y_1;y_2;y_3) \neq (x_1;x_2;x_3)$. In that case we will get the same result, for both triples: $f_B[P(x_1);P(x_2);P(x_3)]=f_B[P(y_1);P(y_2);P(y_3)]$, so in general:

$$\forall\left(x, y \middle| P(x_i) = P(x_i)\right): P\left(f_{A^N}\left[x_1; x_2; x_3\right]\right) = P\left(f_{A^N}\left[y_1; y_2 y_3\right]\right) \tag{7}$$

The process of coarse-graining eliminates degrees of freedom representing local processes without loosing global features of CA evolution. For example, as shown in Fig.6a,b, the rule 128 is the coarse grained version of the rule 146. In [6], the full diagram of coarse graining of all basic 1-D automata was presented. The complex automata (such as rule 110) can be coarse grained only to trivial rules, i.e., 0 and 255. As shown in [18], also the coarse-graining of other rules generating chaotic behavior in 2-D, such as logistic equation, may cause serious

artifacts. Instead of chaotic map, the cascade of reverse bifurcation can be observed behind the accumulation point.

The mapping function $P(.)$ is responsible for information loss. As shown in Fig.7a, only when $S_B=S_A$ no information is being lost, since $P(.)$ is injective. For such S_B, coarse-graining always exists, and it could be easily derived from Eq.(6) because Eq.(7) will be satisfied only for x=y. It turns out, that for $S_B \equiv S_{A^N}$ coarse-graining problem is trivial, so it is reasonable to consider alphabet S_B being much smaller than S_{A^N} (see Fig.7b). As shown in Fig.6c, increasing the alphabet (i.e. assuming that $S_A \subset S_B \subset S_{A^N}$) the fine-scale information can be partially reconstructed.

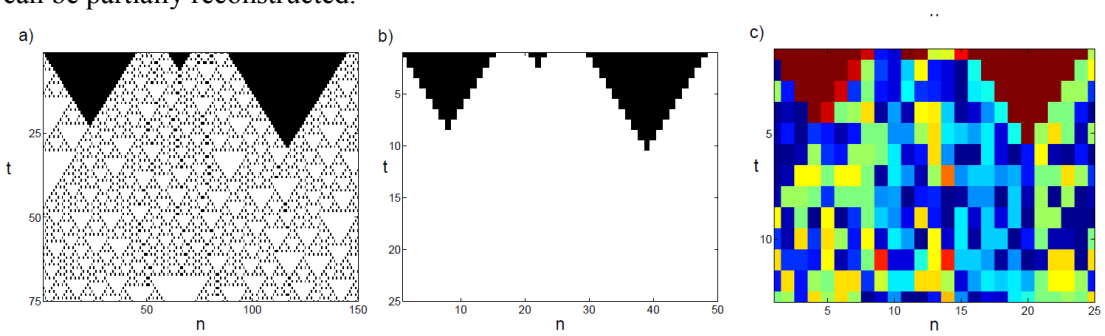

Fig.6 The effect of coarse graining of rule 146 a) the original rule 146 b) its coarse grained version – rule 128, c) coarse grained version of rule 146 using larger alphabet S_B [6].

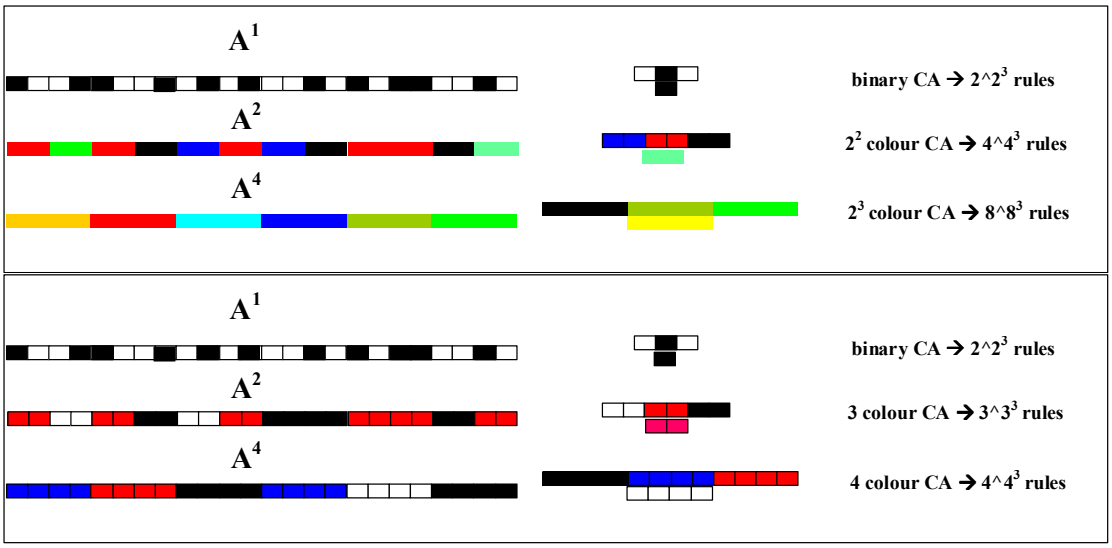

Fig.7 The diagram presenting the process of coarse graining of CA. Information about finer scales can be preserved in new rules, created from greater alphabet than the original one.

The main conclusions can be summarized as follows:

1. Coarse graining of the most of CA to simpler but not trivial automata is possible,
2. Coarse-grained degrees of freedom maybe simple and predictable,
3. Undecidable, chaotic CA cannot be coarse-grained,
4. Finer, physically important DoF, can be incorporated to the coarse-grained model by increasing the alphabet $S_B>S_A$ and changing the rule set.

2.2. Particle method

The Particle method (PM) in its simplistic form, defined by particles interacting with each other via two-body short ranged force (see Eq.1 and Fig.5), can be used directly for

simulation of populations consisting of rather small number of objects. Moreover, the objects must be precisely defined as separate and integrated entities. In such the case, despite the global response of the system is measured in terms of space and time averages, just a local scenario is the focal point of interest. For example, the average speed of crowd flow passing the corridor (see Fig.8a) and its spatial distribution depend on the width of exit door, the existence of crossings, stairs etc. Due to high variability caused by individual behavior, such the simulations should be repeated many times to analyze various possible scenarios. By increasing the number of interacting entities the individual behavior becomes less and less important. The system can be described in terms of stochastic processes and fluctuation-dissipation principles. For example, in the classical molecular dynamics simulations fluctuation of system averages (e.g. kinetic and potential energies) are used to estimate such the important thermodynamic quantities like temperature, pressure, entropy, viscosity, conductivity *etc*. Moreover, an emergent behavior can be observed such as phase separation shown in Fig.8b. By further increase of the number of interacting objects towards to the upper values from the plot in Fig.5, the number of possible scenarios stops growing so fast with the number of objects. The emergent macroscopic behavior, connected with local system anisotropy, begins to dominate over individual and stochastic terms. As shown in Fig.8c, simulating the flow past a plate using more than a million particles and averaging the velocity of particles on a rectangular grid, we can observe the process of eddies formation characteristic for macroscopic flows.

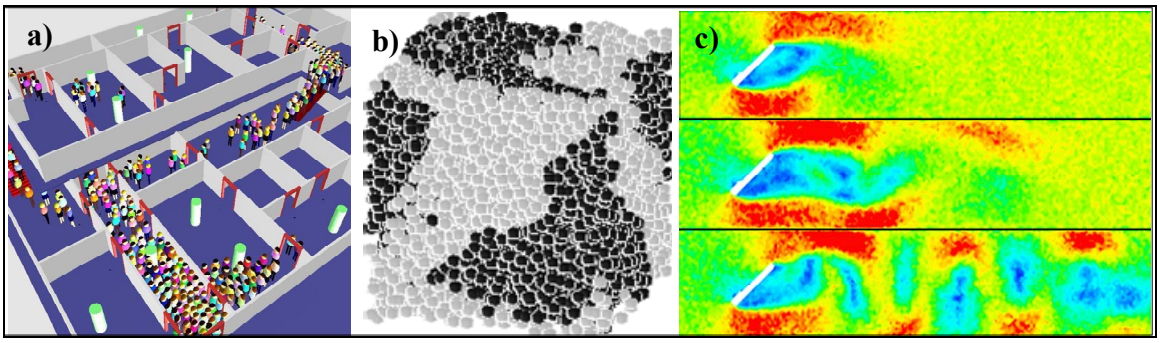

Fig.8 Three types of scenario simulated using PM approach for increasing number of interacting particles: a) crowd simulation may depend strongly on individual motion of a single object [16]; b) phase separation is the emergent effect of stochastic processes (not only) connected with thermal fluctuations; c) flow of one million of particles past a plate mimics macroscopic behavior of fluids.

As was shown in [7, 8, 12], the same computational tool which is used for simulating particle systems in thermodynamic equilibrium, can be generalized easily to enable the simulation of nonequilibrium systems. The simulation of large particles ensembles involving nonequilibrium molecular dynamics (NEMD) provides a consistent microscopic basis for the irreversible macroscopic Second Law of Thermodynamics. The new idea, key to the nonequilibrium development, was the replacement of the external thermodynamic environment by internal control variables. The strong anisotropy of simulation conditions, such as those used for simulation presented in Fig.8c, can be treated as a typical nonequilibrium molecular dynamics scenario.

Because large-scale NEMD simulation can bridge time scales dictated by the fast modes of motion together with the slower modes, which determine the viscosity, it can capture the effects of varying molecular topology on fluid rheology. These effects may come from chemical reactions or mixing with complicated velocity fields. However, in order to capture spatio-temporal scales of micrometers and microseconds occurring, e.g.,in vascular system (see Fig.1), we need billions or more of MD particles simulated in hundred of millions of timesteps [19, 20].

Mesoscopic regimes of this porous system require the fast modes of motion to be coarse grained. At this level, the particles will represent clusters of atoms or molecules, so-called, dissipative particle (DP) [21]. The authors of [21] have shown how to link and pass the averaged properties of molecular ensemble onto DPs by using a systematic coarse-graining procedure. The dissipative particles are represented then by cells defined on the Voronoi lattice with variable masses and volumes (see Fig.9). The Voronoi cells allow for a very clear statement of the problem of coupling continuum equations and molecular dynamics. This is important when the continuum description breaks down in certain regions such as the contact line between two fluids and a solid, or the singularity of the tip in propagating fracture.

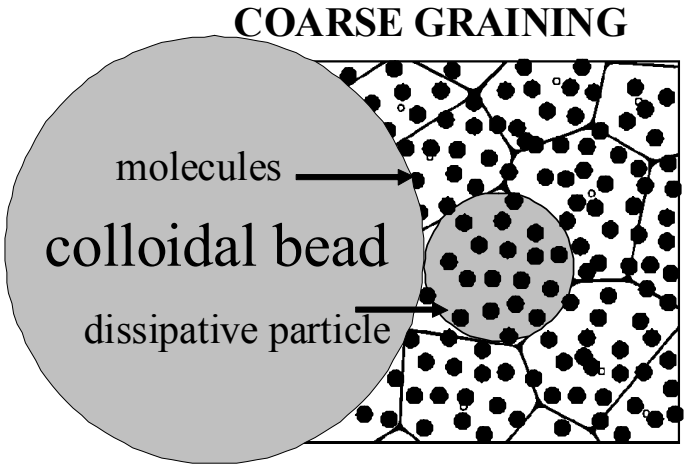

Fig.9. The coarse-graining procedure. The Voronoi cell contains atoms, which are the closest to the cell center. The centers of all the Voronoi cells correspond to the centers of coarse-grained representation of the system - dissipative particles - which can be approximated then by spheres [21].

Entire representation of all the MD particles (atoms or molecules) can be achieved in a general way by introducing an approximation radial function:

$$f_k(\mathbf{r}-\mathbf{r}_k)=\frac{\theta(\mathbf{r}-\mathbf{r}_k)}{\sum_l \theta(\mathbf{r}-\mathbf{r}_l)}, \tag{8}$$

where the positions $\mathbf{r}_k$ and $\mathbf{r}_l$ define the centers of dissipative particles, $\mathbf{r}$ is an arbitrary position, and $\theta(\mathbf{r})$ is the Gaussian function. According to [21], the mass, momentum, and internal energy E_k of the kth dissipative particle are then approximated as:

$$M_k=\sum_i f_k(\mathbf{r}_i), \qquad \mathbf{P}_k=\sum_i f_k(\mathbf{r}_i)m\mathbf{v}_i, \tag{9}$$

$$\frac{M_k U_k^2}{2}+E_k=\sum_i f_k(\mathbf{r}_i)\left(\frac{m\mathbf{v}_i^2}{2}+\frac{1}{2}\sum_{j\neq i}\phi_{MD}(r_{ij})\right)\equiv\sum f_k(\mathbf{r}_i)\varepsilon_i, \tag{10}$$

where $\mathbf{v}_i$ is the velocity of ith MD particle having identical masses m, $\mathbf{P}_k$ is the momentum of the kth dissipative particle, and $\phi_{MD}(r_{ij})$ is the potential energy of the MD particle pair i,j separated by a distance r_{ij}. The particle energy ε_i contains both the kinetic term and a potential term. In order to derive the equations of motion for dissipative particles the time derivatives of Eqs.(10) must be resolved [21]. Finally, after averaging over the velocities, masses and interactions on the Voronoi lattice, we obtain as follows:

$$\frac{d\mathbf{P}_k}{dt}=M_k\mathbf{g}+\sum_l\left\langle\dot{M}_{kl}\right\rangle\frac{\mathbf{U}_k+\mathbf{U}_l}{2}-\sum_l L_{kl}\left(\frac{p_{kl}}{2}\mathbf{e}_{kl}+\frac{\eta}{r_{kl}}\left[\mathbf{U}_{kl}+(\mathbf{U}_{kl}\cdot\mathbf{e}_{kl})\mathbf{e}_{kl}\right]\right)+\sum_l\widetilde{\mathbf{F}}_{kl} \tag{11}$$

where $\mathbf{U}_{kl}$ - relative velocity of dissipative particles *k,l;* p_{kl} - a pressure term between *k* and *l* dissipative particles resulting from conservative MD interactions; L_{kl} - a parameter of the Voronoi lattice; η - the dynamic viscosity of the MD ensemble and the last summation symbolizes the summation over relative fluctuations $\widetilde{\mathbf{F}}_{kl}$ of the coarse-grained representation. This coarse graining procedure links all the forces between the DP to a hydrodynamic description of the underlying molecular dynamics atoms. The method may be used to deal with situations such as this shown in Fig.1 in which several different dynamical length scales are simultaneously present. To increase the computational efficiency, the Voronoi cells can be approximated by spheres (see Fig.9). Using additional simplifications, such as the unification of dissipative particle sizes, we can arrive at a model, which converges to the dissipative particle dynamics (DPD).

In dissipative particle dynamics [22] the two-body interactions between two fluid particles *i* and *j* are assumed to be central and short-ranged. The collision operator, $\Omega\left(r_{ij}, \mathbf{p}_{ij}\right)$, can be defined as a sum of a conservative force $\mathbf{F}_C$, dissipative component $\mathbf{F}_D$ and the Brownian force $\mathbf{F}_B$. The Brownian factor represents the coarse grained equivalence of thermal fluctuations. The equations below show the basic formula describing the two-body forces.

$$\mathbf{F}_C = \pi \cdot \omega\left(r_{ij}\right) \cdot \mathbf{e}_{ij}, \quad \mathbf{F}_D = \gamma \cdot m \cdot \omega^2\left(r_{ij}\right) \cdot \left(\mathbf{e}_{ij} \circ \mathbf{v}_{ij}\right) \cdot \mathbf{e}_{ij}, \quad \mathbf{F}_B = \frac{\sigma \cdot \theta_{ij}}{\sqrt{\Delta t}} \cdot \omega\left(r_{ij}\right) \cdot \mathbf{e}_{ij}$$

$$\omega\left(r_{ij}\right) = \frac{3}{n \cdot \pi\, r_{cut}^{\,2}} \left(1 - \frac{r_{ij}}{r_{cut}}\right) \quad \theta_{ij} \in (-1,1) \text{- } random\ number; n - particle\ \ density \qquad (12)$$

$$\Omega\left(r_{ij}, \mathbf{p}_{ij}\right) = \mathbf{F}_C + \mathbf{F}_D + \mathbf{F}_B \quad \text{for } r_{ij} < r_{cut} \quad \Omega\left(r_{ij}, \mathbf{p}_{ij}\right) = 0 \quad \text{for } r_{ij} > r_{cut}$$

The value of r_{cut} is the cut-off radius which represents the range of interaction between two interacting DP. DPD model with longer cut-off radius reproduces better dynamical properties of realistic fluids expressed in terms of velocity correlation function [23]. Simultaneously, for a shorter cut-off radius, the efficiency of DPD codes increases as $O(1/r_{cut}^{\,3})$, which allows for more precise computation of thermodynamic properties of the particle system from statistical mechanics point of view. A strong background has been provided to DPD in [9,23]. Explicit formulas for transport coefficients in terms of the particle interactions were derived. As shown by Marsh et al. [24], for low value of friction (i.e., γ in Eq.12), low density case and vanishing conservative interactions the interactions between the dissipative particles produce only small deflections. There exist several other methods, which generalize DPD model, e.g., the fluid particle model (FPM) [9] and the thermodynamically consistent DPD (TC-DPD) [10].

One of the serious drawbacks of DPD is the absence of a drag force between the central particle and the second particle orbiting about the first. To eliminate this deleterious effect, the fluid–particle model introduces a non-central force, which is proportional to the difference between the velocities of the particles. In order to bridge mesoscopic with the macroscopic scales using interacting particles, Serrano and Espanol [10] propose a new thermodynamically consistent dissipative particle model (TC-DPD). It uses the principal advantages of the well known SPH (smoothed particle hydrodynamic) scheme, which is a discrete version of the Navier–Stokes equations [26], and includes thermal fluctuations such as in DPD. This model resolves some problems related to the physical interpretation of the original DPD model. The TC-DPD method at present represents a superset for the classical dissipative particle dynamics, fluid particle model and smoothed particle dynamics models [25]. The scale of interest can be easily matched by controlling the size of fluctuation terms. However, the calculation of fluctuation terms in TC-DPD remains very time consuming.

Much simpler method of scale bridging was described in [26]. Coarse-graining in DPD translates to having a number *L* of physical molecules be represented by a single DPD particle. A renormalization or coarse graining is performed that changes the interaction

parameters, but does not change the units. The scaling procedures for number of particles N, mass m, space r_c and time τ units, collision operator parameters (see Eqs.(12) - π, λ, σ) in D-dimensional space are as follows:

$$N' = L^{-1} \cdot N, \quad m' = L \cdot m, \quad r_c' = L^{1/D} \cdot r_c, \quad \tau' = L^{1/D} \cdot \tau,$$
$$\pi' = L^{1-1/D} \cdot \pi, \quad \gamma' = L^{1-1/D} \cdot \gamma, \quad \sigma' = L^{1-1/2D} \cdot \sigma \tag{13}$$

This simple renormalization scheme allows one to scale a DPD-simulation to any desired length scales. The Authors have proved in [26] that DPD is a scale-free method.

Unlike truly discrete cellular automata, the particle method is a discrete-continuum paradigm in which discrete particles evolve in continuous space and time. However, main coarse-graining principles of CA remain very similar to those applied for particle model. Specifically:

1. Both paradigms are homogeneous, i.e., their principles remain the same in every scale. The coarse-grained CA consists of L finer CA, while the fluid particle is made of L interacting MD particles or finer scale DPD particles.
2. The projection $P(.)$ operator (see Eq.(6) and (7)) in CA corresponds to the averaging rule (see e.g. Eq.(8)) in PM.
3. The f_B transition function (new set of coarse-grained CA rules) corresponds to a coarse-grained dissipative collision operator Ω and (like in FPM case) a particle motion scheme.
4. Similarly as f_B compared to f_A (set of CA rules on fine-grained level), the collision operator Ω on the coarse-grained particle level can be more complicated than respective interaction scheme on finer levels. For example, additional non-conservative terms in DPD collision operator, such as dissipative and Brownian forces, can represent averaged DoF from conservative atomistic MD scale. Similarly, the ordinary differential equation of motion (such as in molecular dynamics) can be coarse-grained by more demanding stochastic differential equations.

Summarizing, the coarse-graining of particle method from microscopic (molecular dynamics) to macroscopic (smoothed particle dynamics) formulation is possible, and promotes PM as a robust and homogeneous multi-scale modeling paradigm.

3. Complex automata

The complex automata (CxA) principles were formulated by Hoextra and Sloot [27] [28].. This generalized modeling paradigm encompasses CA, lattice Boltzmann gas (LBG) and Agent Based Models (ABM) techniques as building blocks. Decomposition of the simulated system onto N single-scale cellular automata that mutually interact across many spatio-temporal scales is the key idea of CxA. This decomposition can be performed on the basis of Scale Separation Map (SSM) (an example of SSM is shown in Fig.1) in which each sub-system can be positioned according to its spatial and temporal scales. The processes having well separated spatio-temporal scales can be easily identified as the components of the CxA multi-scale model.

The main problems with CxA model, defined in that way, are its limited feasibility and computability. Even for medium sized systems with two (or three, at most) scales of interest, extraction of a reasonable number of separated regions of interests (ROI), where finer models have to be used, refers to a very restricted number of phenomena such as crack formation [29]. In general, especially in biological systems, the number of ROI involving finer scales and its volume is usually large enough to make the multi-scale simulation extremely demanding (see Fig.2). Having in mind all the computational and formal problems with coupling heterogeneous models representing different scales, the feasibility of developing a truly useful multi-scale biological model remains a dream of the future.

Development of homogeneous, scale invariant modeling metaphors such as CA and PM, in which the scale under interest is identified by the form of collision operator or set of rules, respectively, represents very competitive option to the multi-scale models involving hierarchy of interacting heterogeneous sub-models operating in different scales. It is mainly due to the efficiency, simplicity and generality. As was shown in subsections 2.1 and 2.2, the collision operators and rules in coarse grained models may hold various type of information from finer scales. It allows for creation of supermodels made of a few homogeneous imperfect models carrying complementary knowledge about the simulated system as a whole. As was shown in [30,31], such the supermodel can over perform much more sophisticated multi-scale models and has a nice property of easy data assimilation due to easy coupling of numerical (formal) models with machine learning algorithms. This is because the supermodel approach is methodologically similar to that from machine learning, where ensemble classifier made of simple classifiers become superior over more complex classification algorithms.

As was shown in the previous sections, cellular automata is advantageous over other modeling approaches in simulating systems where interactions between individuals can be represented by a language instead of mathematical equations. Using more rules, i.e., more complicated language, one can simulate finer scales using coarse-grained CA representation (see Fig.6 and 7). The same property holds the particle model. The TC-DPD collision operator in macroscale - much more complicated than conservative MD force in atomistic scales (see [10]) - encapsulates in a consistent way averaged degrees of freedom from atomistic scales represented by Wiener stochastic terms.

Summing up, the particle model reconstructs in a natural way mechanical interactions while cellular automata performs better when information exchange between individuals cannot be described only in terms of positions, velocities and forces. Therefore, by coupling the particle model with cellular automata, one can obtain the possibility to reconstruct both mechanical interactions and finer intercellular processes mimicked by CA rules. This way, the uniform coarse-grained complex automata (CxA) model can describe systems involving multiple scales and, simultaneously, avoiding computationally demanding hierarchy of sub-models.

The CxA consists of the following assumptions representing principal simulation steps.

Assumption 1

The simulated system is made of a set of particles $\Lambda_N=\{O_i\colon O(\mathbf{r}_i,\mathbf{v}_i,\mathbf{a}_i),\ i=1,\ldots,N\}$ where: i - particle index; N - the number of particles, $\mathbf{r}_i,\mathbf{v}_i,\mathbf{a}_i$ - particle position, velocity and attributes, respectively. The vector of attributes $\mathbf{a}_i$ is defined by the particle type, size, and its current state.

Assumption 2

The particle state may depend on time t, concentration of diffusive substances and total pressure exerted on particle i from its closest neighbors.

Assumption 3

The collision operator $\mathbf{\Omega}_i(\ldots)$, which is equal to the sum of particle-particle vector interactions $\mathbf{F}_{ij}(|\mathbf{r}_i-\mathbf{r}_j|,\ \mathbf{v}_i-\mathbf{v}_j,\ \mathbf{a}_i,\ \mathbf{a}_j)$ between the central particle i and all the particles j confined in the sphere of radius r_{cut}, defines the total force acting on particle i. The type of particle-particle interaction, $\mathbf{F}_{ij}$, may depend on the current attributes of particles i and j.

Assumption 4

1. The particle dynamics is governed by the Newtonian laws of motion (see Eqs.(1)). The particle positions are shifted just after computing collision operators acting on every particle i. The Eqs.(1) are integrated numerically in discrete time-steps Δt.
2. The attributes of particles i are updated according to the state of particles in its neighborhood according to prescribed CA rules.

Assumption 5
The particles attributes may also depend on current solutions of other large-scale models formulated in terms of PDEs (partial differential equations) such as reaction-diffusion or hydrodynamics equations.

The following examples show the advantages of CxA metaphor of modeling.

3.1 Flow with a thin layer over a solid surface

The complex type of fluid instability is produced in situations with a thin film falling down inclined plane or a vertical wall. It begins with an excess of fluid flowing from an opened gate placed at the top of a dry wall. This allows the viscous fluid of constant volume V to flow down the wall with a straight contact line (see Fig.10a) that moves according to the direction of the gravitational field. Some time after the fluid release (the time depends on the fluid thickness, viscosity, physical properties of the wall surface), a contact line spontaneously develops and produces a series of fingers of fairly constant wavelengths across the slope (se Fig.10b). This flow is caused by the presence of the contact line, which slows down the film drainage. High pressure near the contact line is responsible for ridge production. According to theory and experiments [32], a perturbed capillary ridge has thicker regions of liquid advancing more rapidly than the thinner regions. The larger resistance at the wedge segments of the finger head or during flow initiation results in larger liquid accumulation and, consequently, increases the subsequent rate of spreading. This also results in an increase in the ridge thickness, detected in the gravity-driven fingering experiments. In the case of complete wetting, intermolecular forces, comparable to the main driving force, are powerful enough to exceed viscous dissipation in a wedge and, hence, overcome this accelerating effect. Thus, the contact line not only increases the resistance to the flow, but also provides an appreciable driving force on the fronts of the falling film.

From this scenario, we proposed in [33] a new 2-D numerical particle model of falling sheet evolution, which can be considered as a supplementary one to the EE theory [32]. Let us consider system of the 1.2×10^5 particles which are initially placed at the top of computational box (see the first snapshot from Fig.10a). This region stands for a vertical wall covered by the particle fluid. The white part of the box represents dry wall. There is not additional supply of fluid to the system. The particle move down in gravitational field according to Newtonian laws interacting with each other via DPD collision operator $\mathbf{\Omega}_{ij}$ (see Eqs.(12)).

The simulation assumptions can be summarized as follows:

- a ridge forms behind the leading edge,
- the ridge has thicker regions of liquid advancing more rapidly than the thinner regions,
- the contact-line resistance plays a "double role" not only in slowing down but also by increasing the rate of spreading.

To fulfill these assumptions we use the following trick, represented in fact by a CA rule. Namely, we assumed that a particle i undergoes large friction force, when the number of particles ***Neigh(i)*** in its vicinity (i.e., within the sphere of radius r_{cut}, see Eqs. (1)) is too small, i.e., when ***Neigh(i)*** < ***Neighmin.*** This particular procedure is shown in Fig.10c. The first equation in Fig.10c represents the discretized and transformed Newtonian equation of particle motion with DPD collision operator $\mathbf{\Omega}_{ij}$ (see Eqs. (1)).
In the original publication [33] we used a little more complicated CA "*if then*" rule, which takes into account the following facts:

1. The fluid falling down an inclined plane is transferred literally into growing lobes at the expense of thinner part of the ridge. Therefore, the fluid behind the ridge is moving faster than that closer to its leading edge.

2. Very thin film of particles can stick to the wall and moves very slowly.

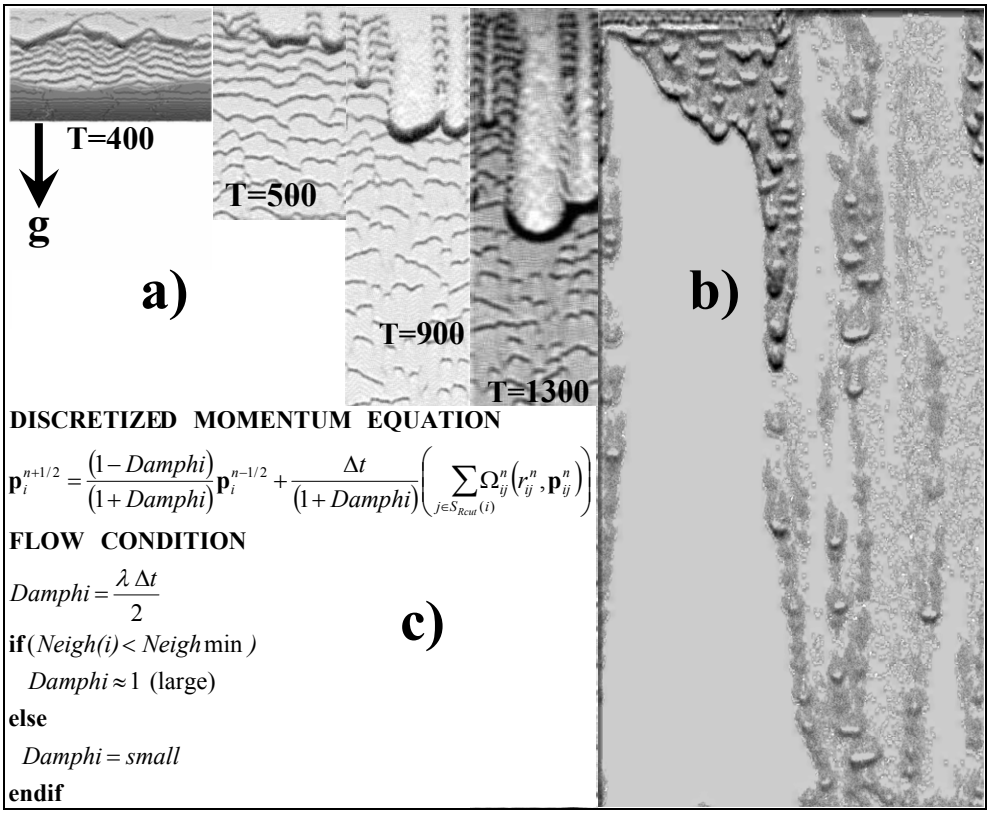

Fig.10. The snapshots from CxA simulations of fluid flow with a thin layer over a solid surface: a) excessive fluid inflow and smooth wall are assumed; b) developed wet pattern of high viscosity fluid on dry and coarse wall; c) the pseudo-code of CxA algorithm.

As shown in Fig.10a,b, the application of this CA rule together with DPD particle dynamics reveal fine-grain structure of this fluid instability such as (see Fig.10a) i.e.,:

1. 3-D "synchronous" (i.e., the neighboring wave fronts are in phase) or "asynchronous" patterns with transverse modulations appear,
2. wave-fronts break-ups (for the "synchronous" case), leading to disordered patterns or "herringbone" patterns to appear in patches (for the "asynchronous" case),
3. spontaneous emergence of avalanches, droplets and rivulets (see Fig.10b).

All of these details are very difficult to simulate within classical fluid dynamical models, due to the critical nature (self-organized criticality) and threshold character of these nonlinear phenomena. Unlike the classical approaches (integrating evolutionary equation [32]), we need not introduce any external and artificial perturbations. All phenomena occur spontaneously due to thermal noise inherent in the nonlinearly interacting particle dynamics. The CxA "*if then*" rule allows for mimicking local scale phenomena such as surface tension and fluid-wall adhesion. Moreover, purely 2-D simulation can mimic the third dimension - fluid thickness - simulated by large particle density variation.

3.2 Tumor growth

The complex automata paradigm can be considerably extended introducing more CxA rules and integrating them with continuous models represented by partial differential equations. Below we present only a brief description of our complex automata model simulating tumor progression. More details can be found in [34-37].

As it is widely known, cancer is one out of major killers in the developed world being responsible for about 20% of deaths in developed countries [38]. Let us skip the complex genetic processes influencing the appearance of the first tumor cells and let us assume that a small cluster of such the cells is ready for proliferation. Typically, further growth of a solid tumor consists of three phases: avascular growth, angiogenesis, vascular growth, metastasis (e.g., [39]).

In avascular phase, the tumor develops due to nutrients diffusion (e.g. O_2) throughout the tissue from neighboring blood capillaries. However, O2 diffusion range is only about 100 μm from the blood vessel thus some of cancer cells are in a chronic shortage of oxygen. Such the hypoxic cells produce and release proteins and other chemical species called tumor angiogenic factors (TAFs) [39]. These signaling compounds diffuse throughout the tissue, and, upon arrival to the blood vessels, they trigger a cascade of events which stimulates the growth of vasculature towards the tumor cluster. In the following phase, vascular one, the tumor having access to unlimited resources of oxygen and other nutrients considerably accelerates its growth. Moreover, through the blood vasculature, the tumor secretes cancerogenic material forming metastases. Thus, whereas in the avascular phase tumors are basically harmless, once they become vascular they are potentially fatal.

As was shown in many papers (e.g. [40,41,42]) computer modeling can allow for answering many principal questions concerning the effects of prescribed chemotherapy or testing new drugs to control the process of tumor growth in all its phases.

There exist many mathematical models of tumor progression in all its phases (e.g. [43-45]). However, only a few consider mechanical factors of growth. Meanwhile, neglecting all microscopic and mesoscopic biological and biophysical processes, tumor growth is a purely mechanical phenomenon. Due to the effect of tumor directional progression, the surrounded tissue, vasculature and tumor on its own undergo continuous process of remodeling. The tissue and vasculature remodeling due to tumor push on is not only the source of pain (e.g., when tumor push on the nerves in the spinal cord) but it influences the speed of its growth as well. Just tumor remodeling is responsible for its heterogeneity, which influences the drug dosage/rate in chemotherapy. Modeling of mechanical growth involves dissipative interactions between normal, cancerous tissues and vascular network. This kind of tumor dynamics could not be reconstructed by using existing models. As shown in [34], CxA can be used as a robust metaphor which closes this gap.

We assume that a fragment of tissue, is made of a set of particles $\Lambda_N=\{O_i: O(\mathbf{r}_i,\mathbf{v}_i,\mathbf{a}_i), i=1,\ldots,N\}$ where: i - particle index; N - the number of particles, $\mathbf{r}_i,\mathbf{v}_i,\mathbf{a}_i$ - particle position, velocity and attributes, respectively. Each particle represents a single cell with a fragment of ECM (extracellular matrix). The vector of attributes $\mathbf{a}_i$ is defined by the particle type {*tumor cell (TC), normal cell (NC), endothelial cell (EC)*}, cell life-cycle state (see Fig. 11a) {*newly formed, mature, in hypoxia, after hypoxia, apoptosis, necrosis*}, cell size, cell age, *hypoxia* time, concentrations of k=TAF, O_2 (and others) and total pressure exerted on particle i from its closest neighbors. The particle system is confined in the cubical computational box with a constant external pressure. For the sake of simplicity the vessel is constructed of tube-like "particles" – EC-tubes – made of two particles connected by a rigid spring (see Fig.11b). We define three types of interactions: particle-particle, particle-tube, and tube-tube. The forces between particles mimic both mechanical repulsion from squashed cells and attraction due to cell adhesiveness and depletion interactions cause by both ECM matrix and the cell. We postulate the heuristics - particle interaction potential $\Omega(d_{ij})$ (Fig.11c) - in the following form:

$$\Omega(d_{ij}) = \begin{cases} a_1 d_{ij}^{\,2}, \text{ for } d_{ij} < 0 \\ a_2 d_{ij}^{\,2}, \text{ for } 0 < d_{ij} < d_{cut} \\ a_2 d_{cut}^{2}, \text{ for } d_{ij} \geq d_{cut} \end{cases} \quad \text{where } a_1 > a_2 \tag{14}$$

where $d_{ij} = |\mathbf{r}_{ij}| - (r_i + r_j)$ and $|\mathbf{r}_{ij}|$ is the distance between particles while r_i and r_j are their radiuses.

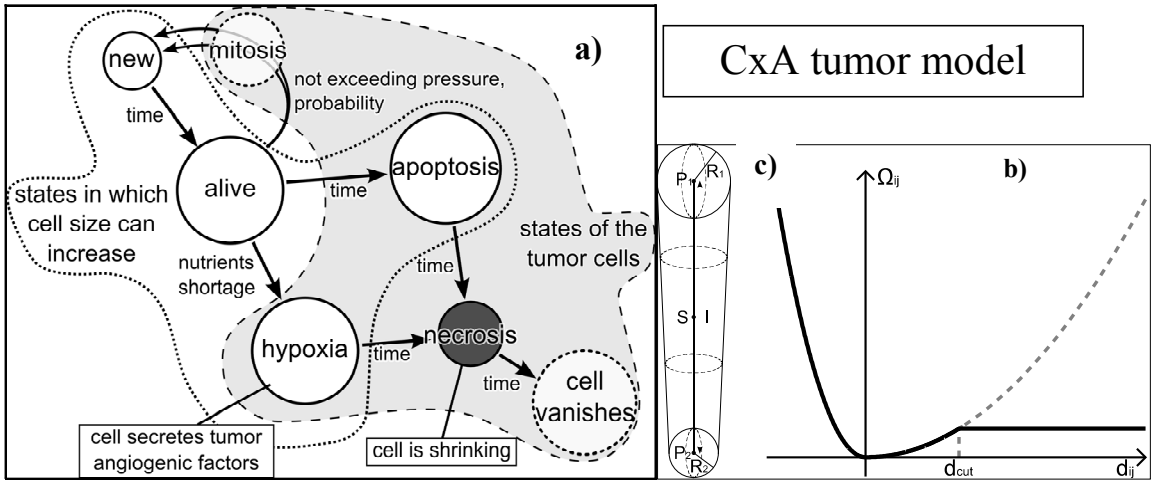

Fig.11. a) Tube-like particle made of two spherical "vessel particles". b) Ω (d_{ij}) – the collision operator. c) The cell life-cycle [37].

We assume that the interactions between spherical particles and EC-tube particles have similar character. However, as shown in [34-37], additional rules have to be introduced to enable appropriate growth of the vascular network. The particle dynamics is governed by the Newtonian laws [Eqs.(1) and DPD collision operator is used for simulating particle-particle interactions.

As shown in Fig.11c, both normal and tumor cells change their states from *new* to *apoptotic* (or *necrotic*). After *mitosis,* well oxygenated cells of certain age and size split into two daughter cells with d_{MIN} diameters. The cell diameter increases proportionally to oxygen concentration up to d_{MAX}. Finally, after given time period, the particles die due to programmed cell death (*apoptosis*). For oxygen concentration smaller than a given threshold, the living cell changes its state to *hypoxia* being the source of TAFs. The cells die and become *necrotic* if they remain in *hypoxia* state too long. We assume that at the beginning, the diameter of *necrotic* cell decreases twice and, after some time, the cell vanishes. This is contrary to apoptotic cells, which are rapidly digested by their neighbors or by macrophages. Both normal and tumor cells differ considerably in duration of the life cycle phases and, especially, in the period of time they can live in *hypoxia*. The *hypoxic* cancerous cells can stay alive a few orders of magnitude longer than normal cells.

The life-cycle for EC-tubes is different. They can grow both in length and in diameter. Reduced blood flow, the lack of VEGF (*vascular endothelial growth factor*), dilation, perfusion and solid stress exerted by the tumor can cause their rapid collapse. Because the EC-tube is a cluster of EC cells, its division onto two adjoined tubes does not represent the process of *mitosis* but is a computational metaphor of vessel growth. Unlike normal and tumor cells, the tubes can appear as tips of newly created capillaries sprouting from existing vessels. The new sprout is formed when the TAFs concentration exceeds a given threshold and its growth is directed to its local gradient.

The distribution of hematocrit is the source of oxygen, while the distribution of tumor cells in *hypoxia* is the source of TAFs. We assume that the cells of any type consume oxygen with the rate depending on both cell type and its current state, while TAFs are absorbed by EC-tubes only. TAFs are washed out from the system due to blood flow.

Because diffusion of oxygen and TAFs through the tissue is many orders of magnitude faster than the process of tumor growth, we assume that both the concentrations and hydrodynamic quantities are in steady state in the time-scale defined by the time-step of

numerical integration of equations of motion. To calculate the concentrations of oxygen and TAF we solve the reaction-diffusion equations numerically by using approximation theory. One can estimate a function *f* at position **r** by using smoothing kernels *W* as follows:

$$f(\mathbf{r}) = \sum_{j=1}^{n} m_j \frac{f_j}{\rho_j} W(\mathbf{r} - \mathbf{r}_j, h) \tag{15}$$

where m_j is the mass, $\mathbf{r}_j$ is the position, ρ_j is the density and f_j is the quantity *f* for neighbor particle *j*, respectively. Here, *n* is the number of neighboring particles within cut of radius *h* ($|\mathbf{r} - \mathbf{r}_j| \le h$). When $\mathbf{r}=\mathbf{r}_i$, $f(\mathrm{r})$ is denoted by f_i. The smoothing kernel approximates a local neighborhood **r** within distance *h*. Thus, we can estimate the density ρ_i for a particle *i* at location $\mathbf{r}_i$ by:

$$\rho_i = \sum_{j=1}^{n} m_j W(\mathbf{r}_i - \mathbf{r}_j, h) \tag{16}$$

where *j* is the index of the neighboring particle. The kernel should be smooth, symmetric and satisfy the following equation:

$$\int_{\Omega} W(\mathbf{r}, h) d\mathbf{r} = 1 \tag{17}$$

We used 3D *poly6* kernel proposed by Muller et al. [51].

$$W_{poly6}(\mathbf{r}, h) = \frac{315}{64\pi h^9} \begin{cases} (h^2 - |\mathbf{r}|^2)^3 & |\mathbf{r}| \le h \\ 0 & \text{otherwise} \end{cases} \tag{18}$$

We selected this kernel due to its simplicity. As shown in [51], better kernels can be used, however, at the cost of computational efficiency. The Laplacian can be approximated then:

$$\Delta f_i = \sum_{j=1}^{n} \frac{m_j}{\rho_j} f_j \cdot \Delta W(\mathbf{r}_i - \mathbf{r}_j, h) \tag{19}$$

Substituting Laplacian in the reaction-diffusion equation by Eq.(8) we got the following expression for concentrations c_i^K of $K=\{oxygen,\ TAF\}$ in particle *i* (χ^K – reaction factor). When *K=oxygen*, then *I=TAF* and vice versa.

$$c_i^K = \frac{\left(\frac{\chi_i^I c_i^I}{D} - \sum_{j=1, i \ne j}^{n} \frac{m_j}{\rho_j} c_i^K \cdot \Delta W(\mathbf{r}_i - \mathbf{r}_j, h) \right)}{\left(\frac{m_i}{\rho_i} \Delta W(0, h) - \frac{\chi_i^K}{D} \right)} \tag{20}$$

By solving this equation iteratively in each time-step of Newtonian equation integration, we got approximate concentration of TAF and oxygen in each particle location.

The particles are confined in the cubical computational box of volume *V*. Because the average kinetic energy in the system is negligible small, from the virial theorem we obtain that:

$$P \approx \frac{1}{3V} \cdot \sum_{i<j}^{N} \mathbf{F}_{ij} \circ \mathbf{r}_{ij} \ . \tag{21}$$

The internal pressure increases due to increasing number of particles (cells). The increase of box volume *V* compensates the pressure increase above a given threshold.

On the other hand, the blood circulation is slower than diffusion but still faster than *mitosis* cycle. These facts allow for employing fast approximation procedures for both calculation of blood flow rates in capillaries and solving reaction-diffusion equation (see [34]). After initialization phase, in subsequent time-steps we calculate forces acting on particles, new particle positions, the diffusion of active substances (nutrients, TAFs, pericytes), the intensity of blood flow in the vessels and the states of individual cells triggered by previous three factors and constrained by time clocks of individual cells. All of these modifications of cell states may result in cell *mitosis* or its death. They can also change some cell functions (e.g. those under *hypoxia*) their size and environmental properties (e.g., cancerous cells can secrete acid to eliminate neighboring tissue cells).

Summing up the basic procedures of our CxA particle model consist of: the model initialization phase, i.e., definition of initial and boundary conditions, and its evolution driven by the following phenomena:

a. Newtonian dynamics of interacting cells,
b. diffusion of oxygen and TAF,
c. cellular life cycle modeled by CxA rules,
d. vessels sprouting and growth,
e. vessels remodeling due to blood flow, vessel maturation and degradation.

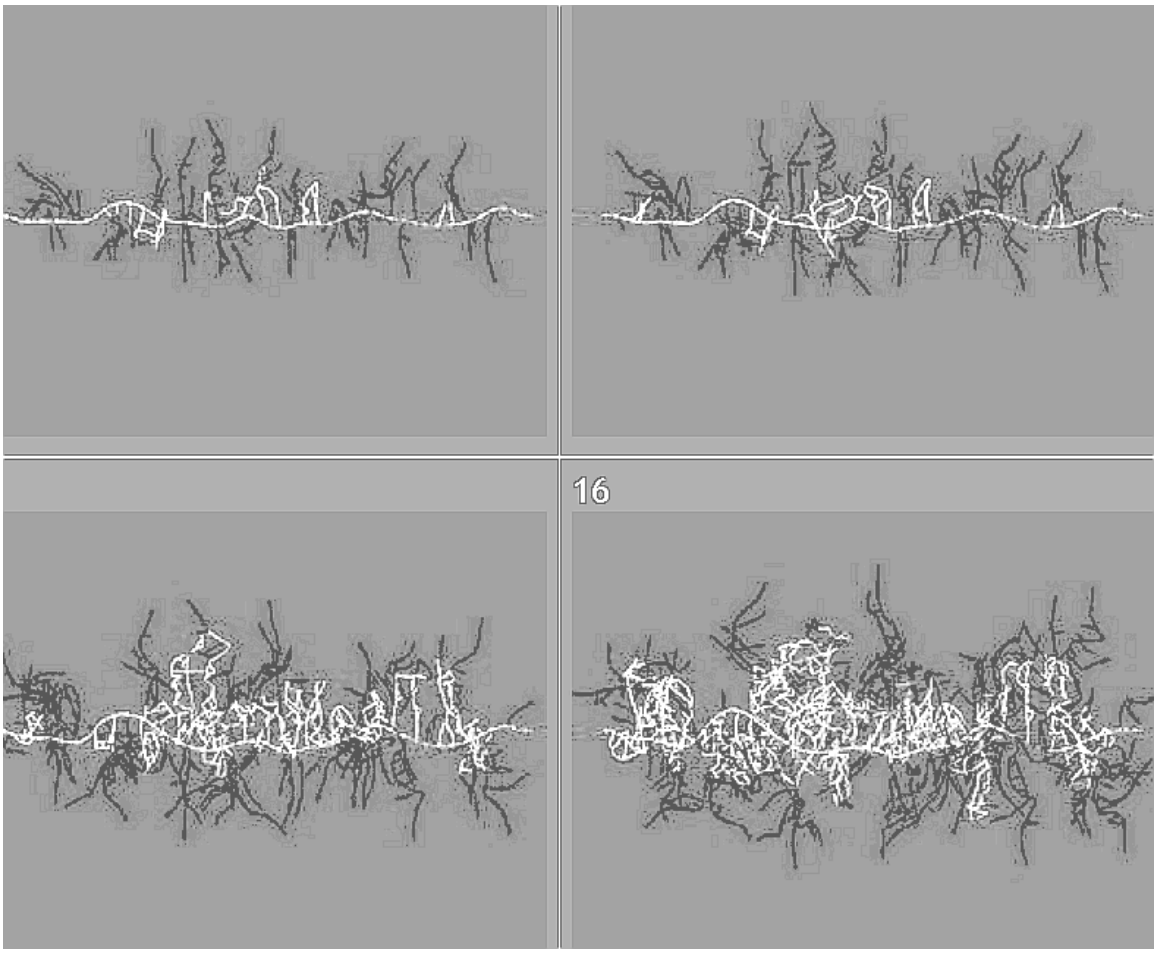

Fig.12 The snapshots from 3-D CxA simulation displaying development of vasculature due to angiogenesis. The white network represents functional blood vessels while the black one shows non-functional vessels. Initially, the single vessel passes throughout the tumor. The tumor cells are invisible in this figure.

As shown in Fig.12, the straight blood vessel which is passing initially throughout cancerous tissue, begin to sprout out. The newly created lumen become functional, i.e., is able to transport blood, when a loop (anastomosis) with another functional vessel creating pressure gradient is formed. Moreover, the capillary has to be covered with adequate quantity of mural cells. Mural cells are vascular support cells that range in phenotype from pericytes to vascular smooth muscle cells [46]. As displayed in Fig.12 and 13, the structures of vasculature become very complex and dynamic due to continual vessels maturation and degradation. The newly created vasculature inside the tumor is unstable, vulnerable to rapid changes in blood pressure caused by the lack of previously mentioned factors and mechanical remodeling (see Fig.13).

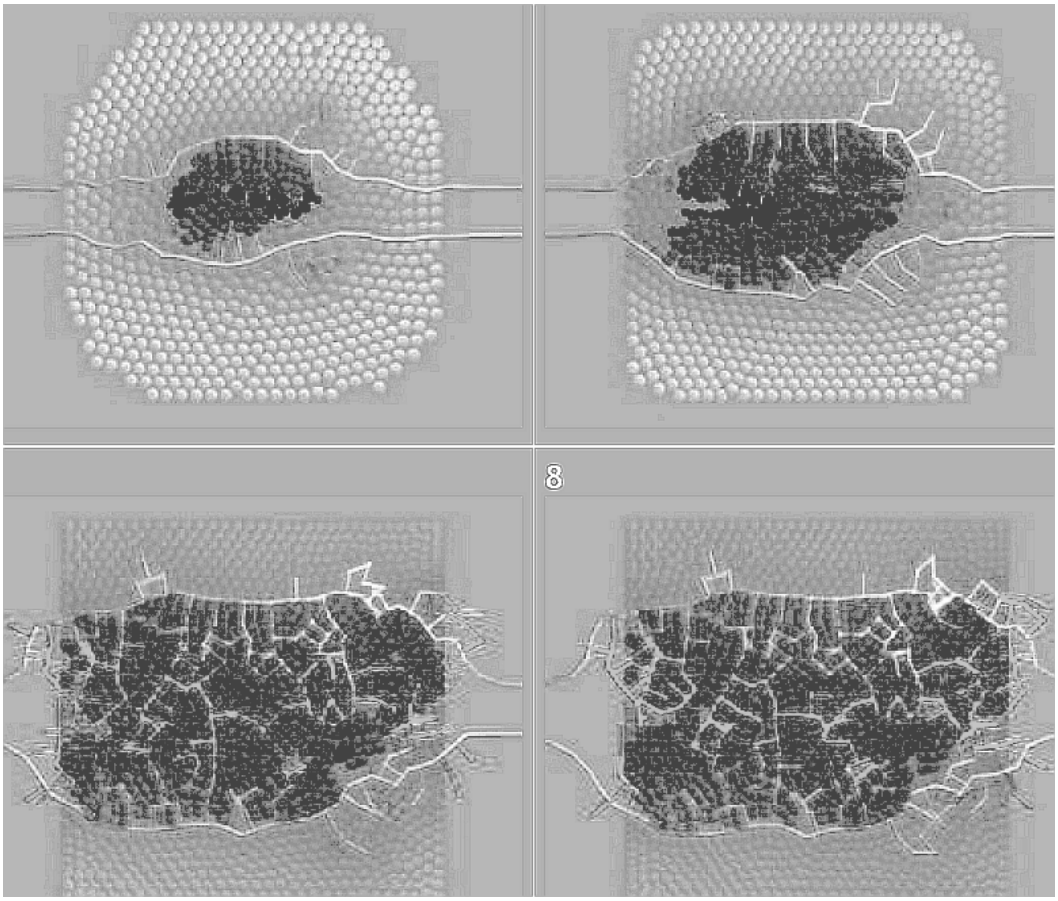

Fig.13. The snapshots from 2-D CxA simulation of tumor growth and vascular network remodeling.

Very similar CxA model can be applied for simulation of cereal infection by parasite fungi called *Fusarium Graminearum* (Fg). In the following section we present preliminary results of modeling Fg infection.

3.2 *Fusarium Graminearum* invasion

Fusarium graminearum is one of the main causal agents of *Fusarium* head blight (FHB) infection. It attacks cereal crops what results in significant losses. The epidemic, which took place in North America from 1998 to 2000, costs almost $3 billion. Another effect of this plague is the contamination of grain with mycotoxins, which is extremely harmful for animals and humans.

Wheat heads are the most susceptible to infection during anthesis. Other factors favoring infection are high humidity and temperature [47]. Initially, the fungus does not penetrate the epidermis. As shown in [47,48], at this stage it develops on the external

surfaces of florets and glumes and grows towards susceptible sites within the inflorescence. Other roads of colonization of internal tissue include stomata and underlying parenchyma, partially or fully exposed anthers, openings between the lemma and palea of the spikelet or floret during dehiscence and through the base of the wheat glumes where the apidermis and prenchyma are thinwalled [47,48]. As every model is a metaphor of some real phenomenon the following assumptions were made:

1. Every *Fusarium* and plant cell is a particle interacting with the other particles.
2. Every cell has a number of attributes that evolve in time.
3. The concentration of nutrients is uniform in a single cell and constant in the specific time step.
4. Nutrients circulation in the fusarium body, which allows *Fusarium* to proliferate, is the effect of diffusion.
5. Each *Fusarium* and plant cell is in one of three discrete states which models cell-life cycle.

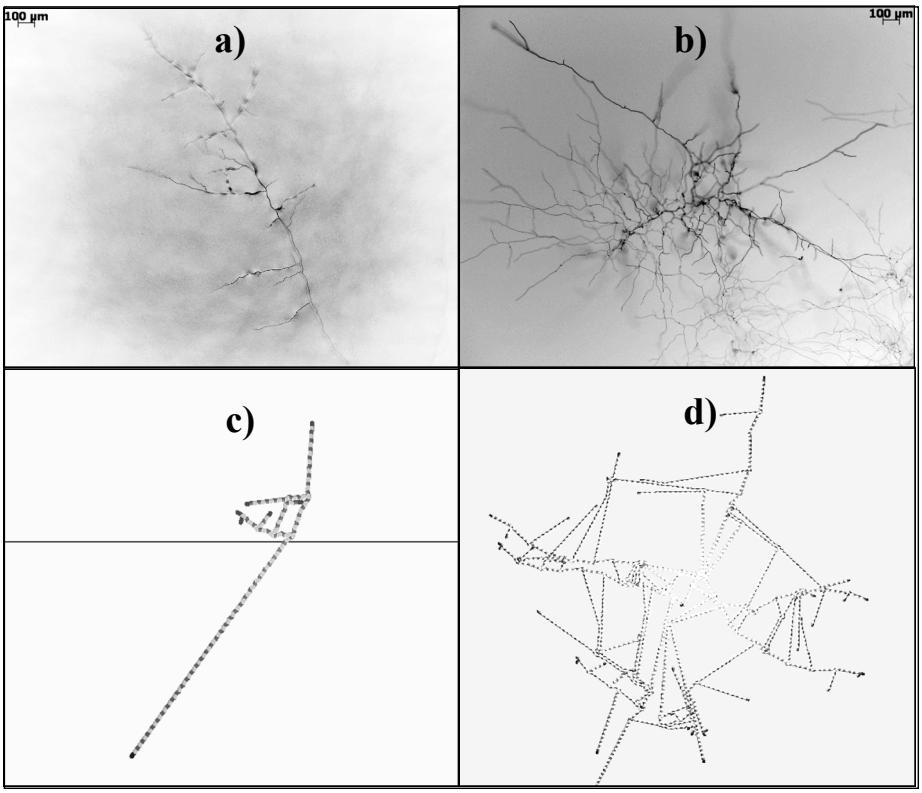

Fig.14 The snapshots from development of *Fusarium* in SNA (nutrient poor) a,c and PDA (nutrient rich) b,d environment from experiment (a,b) (courtesy of Dr Shea Miller, Agriculture and Agri-*Food* Canada, ECORC, *Ottawa*) and simulation using CxA (c,d). In c) *Fusarium* does not branch at all in the nutrients-poor environment below the horizontal black line. It starts to develop more extensively only after reaching the nutrients rich half space above the black line.

The laboratory experiments from Fig.14 a,b were conducted *in vitro* in artificial conditions. This means that no nutrients were produced in the course of experiments and the initial amount of food was only consumed by *Fusarium*. They were performed on flat surfaces on the so called Petri dishes. Two types of environment were tested: SNA, which is nutrient-poor and PDA, which is nutrient-rich. Both substances are water solutions. This allows for two important assumptions: the fungus does not encounter much strain from the environment and diffusion does not need to be modeled directly. We may safely assume that the diffusion in water is fast enough to keep uniform nutrients concentration in the whole volume. As a result

all fungus cells have identical external nutrients level and there is also no need to model diffusion inside the fungus. In this early modeling stage only model of the hyphae growth and physical behavior has been developed. Due to the absence of plant cells in real experiments interactions with environment were not modeled.

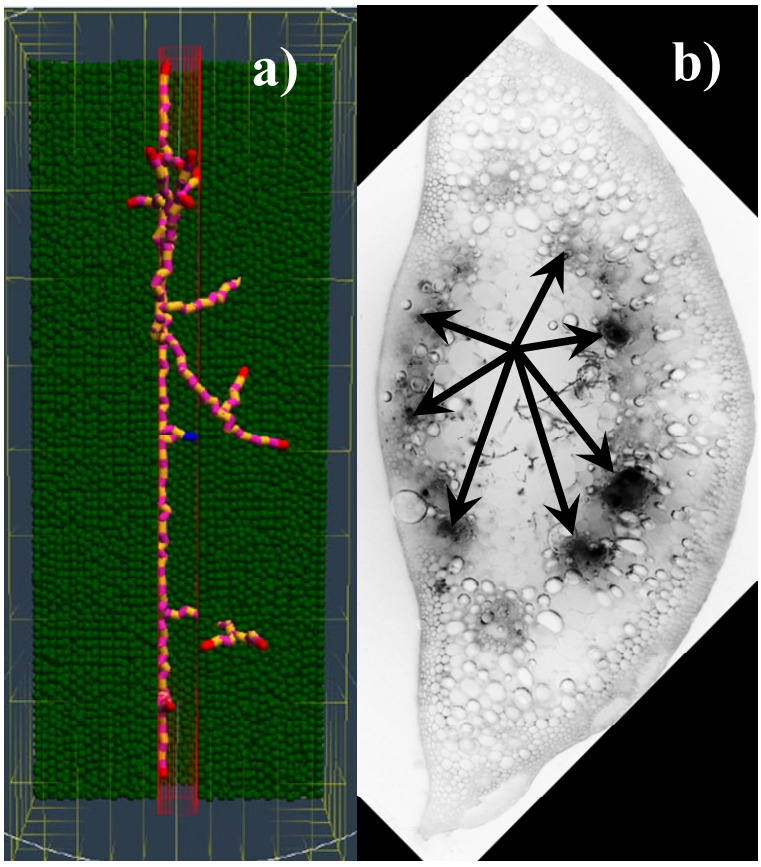

Fig.15. The development of *Fusarium* in vascular bundles and rachis - nutrient poor environment: a) vertical growth simulated using CxA; b) microscopic image of the cross section throughout the stem of wheat head showing *Fusarium* (black stains pointed by arrows) penetrating the rachis (courtesy of Dr Margaret Balcerzak, Agriculture and Agri-*Food* Canada, ECORC, *Ottawa*).

As shown in Fig.14, the confrontation of simulation results with experimental data is cautiously optimistic. The qualitative character of growth is very similar. However, the structural characters of networks produced by *Fusarium graminearum* and simulation code are clearly different. This can be improved, however, by using higher resolution and playing the parameters responsible for the sprouting phenomenon. Another confrontation of simulation with experiment, displayed in Fig.15, once again shows good qualitative agreement of the two. Fg spreads mainly through vascular bundles, penetrating also the closest neighborhood. In the case when fungi find the nutrient rich part of the plant, it changes the growth type from linear (Fig.14 a,c) to extensive one (Fig.14 b,d), devastating it completely.

4. Conclusions and discussion

The most of biomedical problems, which concentrates on finding remedies against a pathogen expansion, are extremely difficult to simulate. Mainly due to the lack of:

- adequate numerical approaches representing many spatio-temporal scales involved in biological processes, their discrete nature and high nonlinearity;
- the procedures and practices of coupling numerical models with diverse sources of data.

The development of integrated computational models and data coupling procedures is a vital problem in computational sciences, which considerably postpones the successful implementation of computational techniques in biosciences.

We have introduced here a novel modeling concept, called Complex Automata, which integrates the two types of modeling techniques, namely, Particle Method and Cellular Automata. The particle represents here both the component of a dynamical system and plays the role of CA node. We have demonstrated that the multi-scale modeling techniques can be built upon the notion of coarse graining of these two approaches. Instead of developing complicated multi-scale models which consist of many submodels representing various scales coupled by a scales-bridging mechanism, we propose here a uniform, single scale, coarse grained computational framework for which information about finer scales is inscribed in CA rules and particle interactions.

Both the CA rules and the PM collision operator can be matched to the scale under interest by removing or inserting additional degrees of freedom. The number of DoF can be manipulated by changing complexity of particle interactions and by increasing the set of CA rules. The most important advantage of such the approach over other classical multi-scale models is that the spatio-temporal scale considered remains as coarse as possible, while the finer scales are simulated by more complex collision operator and CA rules.

We have shown that the particle method decides about the mechanical properties of the system. Microscopic phenomena involving fluctuations and dissipative behavior can be added in a consistent way exploiting widely known modeling techniques such as DPD or TC-DPD. We demonstrated that some other physical properties, like surface tension, can be simulated by introducing to the interaction model a simple CA rule. Apart from system properties resulting from simple Newtoniam mechanics, other microscopic biological processes can be encapsulated in CA rules. These rules depend on the current configuration of the nearest neighbors and other phenomena, e.g., described by the continuum fields obtained from integrating PDEs.

We have also presented a proof-of-concept of our approach by employing CxA as a metaphor in modeling of two different biological phenomena. The ability of mimicking both mechanical interactions of tumor with the rest of tissue and penetration properties of *Fusarium graminearum,* shows that our model can reproduce realistic 3-D dynamics of these complex biological systems.

For identification of weak points of these (i.e., cancer proliferation and *Fg* infection) and similar pathogens, the contemporary biology employs a bottom-up approach. Manipulation of the level of expression of solitary genes allow for controlling molecular pathways which influence some phenotype behaviors. However, to explain a complex biological phenomenon involving many genes, this process remains very inefficient, expensive and unreliable. The solution space inflates exponentially with the number of genes making impossible to find respective genetic code. We hypothesize that top-down approach exploiting numerical modeling empowered by data assimilation procedures enables more precise selection of these molecular triggers. It can serve as a bidirectional coupling factor between genotype and phenotype.

The general concept of data assimilation with CxA model could be formulated as follows. On the base on observed phenotypic behaviors we can categorize them (e.g. using microscopic images) and associate these categories to genotypes extracted from experimental data (e.g., microarrays) by using machine learning and data analysis tools. On the other hand, running the coarse-grained numerical model (level 1) one can adjust the sets of parameters of the model to the respective phenotype categories. The parameters are associated with some microscopic biochemical processes, which can be scrutinized in molecular level, i.e., much closer to the genotype than emergent phenotypic behavior. To make the prediction more

accurate, one can run fine-grained (level 2) model with extended collision operator and larger set of CA rules. The new set of parameters is matched to the data by using previously obtained (level 1) parameters. This procedure can be applied downscale. The concept of data assimilation is being developed now and will constitute the following step in devising reliable data driven CxA models.

We expect that with such the advancement in modeling techniques, new faster and cheaper methods will be developed which allow for attacking biological problems in a more systematic and focused way.

Acknowledgements This research is financed by the Polish Ministry of Higher Education and Science, project NN519 579338 and partially by AGH grant No.11.11.120.777. The Author thanks Professor AZ Dudek from Division of Hematology, Oncology, and Transplantation at the University of Minnesota, dr. Shea Miller and Margaret Balcerzak from Agriculture and Agri-Food Canada (AAFC), Ottawa for discussions about mediacal and biological aspects of this work, respectively. Thanks are also due to Mr Przemysław Głowacki and dr Rafał Wcisło for their contribution to this paper.

References

1. Dzwinel W, Yuen DA, Boryczko K, Bridging diverse physical scales with the discrete-particle paradigm in modeling colloidal dynamics with mesoscopic features, *Chemical Engineering Sci*., 61, 2169-2185, 2006.
2. Vasilyev OV, Bowman K., Second-Generation Wavelet Collocation Method for the Solution of Partial Differential Equations, *Journal of Computational Physics*, 165/2, 660-693, 2000.
3. Vasilyev OV, Zheng X, Dzwinel W., Dudek AZ, Yuen DA, Collaborative Research: Virtual Melanoma – A Predictive Multiscale Tool for Optimal Cancer Therapy, NiH proposal, 2011 unpublished.
4. Wolfram S., *A New Kind of Science* (Wolfram Media Incorporated, 2002), p. 1263.
5. Chopard B and Droz M, *Cellular Automata Modeling of Physical Systems* (Cambridge University Press, 1998).
6. Israeli N., Goldenfeld N, Coarse-graining of cellular automata, emergence, and the predictability of complex systems, *Phys. Rev. E,* 73/2, 026203, 2006.
7. Dzwinel W, Alda W, Yuen DA., Cross-Scale Numerical Simulations Using Discrete-Particle Models, *Molecular Simulation*, 22, 397-418, 1999.
8. Dzwinel W, Alda, W, Kitowski J., Yuen, DA., Using discrete particles as a natural solver in simulating multiple-scale phenomena, *Molecular Simulation*, 20/6, 361-384, 2000.
9. Espanol P, Fluid particle model. *Phys Rev E*, **57**, 2930-2948, 1998.
10. Serrano M., Espanol P, Thermodynamically consistent mesoscopic fluid particle model. Physical Review E 64/4, 046115, 2001
11. Beazley DM., Lomdahl PS., Gronbech-Jansen N, Giles R and Tomayo P, Parallel Algorithms for Short Range Molecular Dynamics, In: *World Scientific* s *Annual Reviews of Computational Physics III,* 119- 175, 1996.
12. Dzwinel W, Alda W, Pogoda M, Yuen DA, Turbulent mixing in the microscale, *Physica D*, 137, 157-171, 2000.
13. German TC, Kadau K. Trillion-Atom Molecular Dynamics Becomes a Reality, *International Journal of Modern Physics C*, 19/9, 1315-1319, 2008
14. Dzwinel W, Virtual Particles and Search for Global Minimum, *Future Generation Computer Systems*, 12, 371-389, 1997
15. Pelechano N and Badler NI, Improving the Realism of Agent Movement for High Density Crowd Simulation, http://www.lsi.upc.edu/~npelechano/MACES/MACES.htm

16. Helbing D, Farkas IJ, Vicsek T, Simulating Dynamical Features of Escape Panic, *Nature*, 407, 487-490, 2000.
17. Nigiel G. *Agent-based Models*, Sage Publications: London, 2007 pp.100
18. Dzwinel W., Spatially extended populations reproducing logistic map*, Central European Journal of Physics*, 8/1, 33-41, 2010.
19. Nakano A, Bachlechner M, Campbell T, Kalia R, Omeltchenko A, Tsuruta K, Vashishta ., Ogata S, Ebbsjo I, Madhukar,A, Atomistic simulation of nanostructured materials. *IEEE Computational Science and Engineering* 5 (4), 68–78, 1998.
20. Nakano A, Bachlechner ME, Kalia RK, Lidorikis E, Vashishta P, Multiscale simulation of nanosystems. *Computing in Science and Engineering* 3/4, 42–55, 2001.
21. Flekkoy EG, Coveney PV, Foundations of dissipative particle dynamics. *Physics Review Letters* 83, 1775–1778, 1999.
22. Hoogerbrugge PJ, Koelman JMVA.. Simulating microscopic hydrodynamic phenomena with dissipative particle dynamics, *Europhysics Letters* 19 (3), 155–160, 1992.
23. Espanol P, Serrano M, Dynamical regimes in DPD, *Physical Review E*, 59/6, 6340–6347.
24. Marsh C, Backx G. Ernst MH, Static and dynamic properties of dissipative particle dynamics. *Physical Review E 56*, 1976, 1997.
25. Libersky LD, Petschek AG, Carney TC, Hipp JR, Allahdadi F.A, High strain Lagrangian hydrodynamics, *Journal of Computational Physics*, 109/1, 67–73, 1993.
26. Fuchslin RM, Eriksson A, Fellermann H, and Ziock H-J, Coarse-Graining and Scaling in Dissipative Particle Dynamics, *J. Chem. Phys.* 130, 214102, 2009.
27. Hoekstra AG, Lorenz E, Falcone LC, Chopard B, Towards a complex automata framework for multi-scale modeling: Formalism and the scale separation map, *Lect Notes Comput Sci*, 4487, 922-930, 2007
28. Sloot PMA, Kroc J, Complex Systems Modeling by Cellular Automata", Encyclopedia of Artificial Intelligence, Ed. Rabunal JR, Rabunal Dopico JR, Dorado J, Sierra AP, Informatio SCI, Harshey-New York, 353-360, 2009.
29. Abraham F, Broughton J, Bernstein N, Kaxiras E, Spanning the length scales in dynamic simulation, *Computers in Physics* 12/6, 538–546, 1998.
30. Berge van den LA, Selten FM, Wiegerinck W, and Duane GS, A multi-model ensemble method that combines imperfect models through learning, *Earth Syst. Dynam.*, 2, 161-177, 2011
31. The web page of SUMO EU FET project, http://www.knmi.nl/samenw/sumo/news.html
32. Oron A, Davis SH and Bankoff SG, Long-scale evolution of thin films", *Rev. of Modern Phys.* 69(3), 931-980, 1997
33. Dzwinel W, Yuen DA, Dissipative particle dynamics of the thin-film evolution in mesoscale, *Molecular Simulation*, 22, 369-395, 1999
34. Wcisło, R., Dzwinel, W., Yuen, D.,A., Dudek, A..Z., 2009, "A new model of tumor progression based on the concept of complex automata driven by particle dynamics", J. Mol. Mod*,* 15, no.12, 1517–1539.
35. Wcisło R., Dzwinel, W., Particle Model of Tumor Growth and Its Parallel Implementation, *Lecture Notes in Computer Science*, PPAM, Wrocław, 13-16 September 2009, LNCS, 322-331, 2010
36. Wcisło R, Dzwinel W, Particle based model of tumor progression stimulated by the process of angiogenesis, *Lectures Notes in Computer Science,* ICCS 2008, *LNCS* 5102, pp 177-186. 2008
37. Wcisło R, Gosztyła P, Dzwinel W, N-body parallel model of tumor proliferation, SCSC 2010, Proceedings of Summer Computer Simulation Conference, July 11-14, 2010, Ottawa, Canada, p 160-167.
38. Jemal A, Siegel R, Jiaquan Xu, Ward E, Cancer Statistics 2010, *CA Cancer J Clin*. 60:277-300, 2010.

39. Folkman, J., Tumor angiogenesis, Therapeutic implications, *N Engl J Med*, 285, 1182-1186, 1971.
40. Castorina, P., Carcò, D., Guiot, C., Deisboeck, T.S., 2009, "Tumor Growth Instability and Its Implications for Chemotherapy", Cancer Res, 69, no.21.
41. Lowengrub, J.S., Frieboes, H.B., Jin, F., Chuang, Y-L., Li, X., Macklin, P., Wise, S.M., Cristini, V., 2010: "Nonlinear modelling of cancer: bridging the gap between cells and tumours", Nonlinearity, 23, R1-R91.
42. Bellomo, N., de Angelis, E., Preziosi, L., 2003, "Multiscale Modeling and Mathematical Problems Related to Tumor Evolution and Medical Therapy", J Theor Med.. 5, no.2, 111–136.
43. Chaplain, M.A.J., 2000, "Mathematical modelling of angiogenesis", J Neuro-Oncol, 50, 37–51.
44. Preziozi, L. (ed), 2003, Cancer modelling and simulation. Chapman & Hall/CRC Mathematical Biology & Medicine.
45. Mantzaris, N., Webb, S., Othmer, H.G., 2004, "Mathematical Modeling of Tumor-induced Angiogenesis", J Math Biol., 49, no.2, 1432-1416.
46. Raza A, Franklin MJ, Dudek AZ., Pericytes and vessel maturation during tumor angiogenesis and metastasis, *Am J Hematol.,* 85(8), 593-8, 2010
47. Brown NA, Urban M, van de Meene AML, Hammond-Kosack KE, The infection biology of *Fusarium graminearum*: Defining the pathways of spikelet to spikelet colonisation in wheat ears, *Fungal Biology*, 114/7, 555-571, 2010.
48. Miller SS, Chabota DMP, Ouellet T,, Harrisa LJ, Fedak G, Use of a Fusarium graminearum strain transformed with green fluorescent protein to study infection in wheat (Triticum aestivum), *Canadian Journal of Plant Pathology*, 26/ 4, 453-463, 2004.